Materials Today: Proceedings 41 (2021) 479–489

Contents lists available at ScienceDirect

Materials Today: Proceedings

journal homepage: www.elsevier.com/locate/matpr

Metal organic framework for sensing toxic metal ions in water

M.S. Sreevidya [a], Rani Pavithran [b,*]

[a] Department of Chemistry, University College, Thiruvananthapuram 695034, India
[b] Central Polytechnic College, Vattiyoorkkavu, Thiruvananthapuram 695013, India

ARTICLE INFO

Article history:
Received 4 May 2020
Accepted 9 May 2020
Available online 29 May 2020

Keywords:
Hetero bimetallic metal organic framework
Solvothermal synthesis
Heavy metal ions
Sensing capability
Zirconium
Benzene-1,4-dicarboxylic acid

ABSTRACT

Hetero bimetallic metal organic framework (MOF) of zirconium, and copper has been synthesized using benzene-1,4-dicarboxylic acid (BDC) as the linker by solvothermal synthesis. The MOF has been characterized using FT-IR, powder XRD, FE-SEM, EDAX, TEM, TGA, UV and PL analysis. Also the sensing capability of the MOF has been investigated using different concentrations of toxic metal ions like lead (II) and chromium (VI).

Selection and peer-review under responsibility of the scientific committee of the International Conference on Energy and Environment.

1. Introduction

Water quality and scarcity are of growing global concern in the twenty-first century. Pollution from mines, factories or even poorly constructed water supply pipes lead to devastating effects on the environment and vital biological processes, including human health. Lead is one of the highly ranked most dangerous heavy metals due to its toxicity [1]. Chromium, especially chromium (VI), is one of the most common toxic heavy metal pollutants present in water. Chromium causes permanent damage to human health and living environment, even at a low concentration [2]. Effective detection and removal of toxic heavy metal ions (Hg^{2+}, Pb^{2+}, Cd^{2+}, etc.) from water sources are paramount to regions spanning the globe. The efficient, straightforward, and real-time detection of trace amounts of these toxic metal ions are of great importance in global health and environmental concerns [3]. Up to now, the prevailing detection of these heavy metal ions is based on instrumental methods, including atomic absorption spectroscopy, ICP-MS (inductively coupled plasma mass spectrometry) and electrochemical analysis [4]. However, these methods are often time-consuming, expensive and hardly portable and require trained personnel. Therefore, development of a new convenient, reliable and inexpensive method for the detection of heavy metals in water is the need of the hour [5].

Metal organic frameworks (MOFs) have attracted great interest, with impressive properties and wide potential applications. In particular, the MOF-based chemical sensor is clearly a promising platform for chemical sensing [6]. MOFs formed by the combination of metal centers or clusters with organic linkers, have gathered immense attention not only due to their intriguing architectures rendered by a variety of bridging ligands and metal ions but also their potential application in gas storage, separation, catalysis, proton conduction, sensing, and so on [7–9]. Recently, luminescent sensing with MOF materials has been considered as one of the most promising technologies for chemical and biological detection applications because it provides a simple, sensitive, selective, and economical approach for online monitoring of target analytes without complicated sample pretreatments [10].

Herein, we present a bimetallic MOF $[Zr/Cu(1,4\text{-BDC})(H_2O)]_n$ whose sensing capability has been investigated using different concentrations of toxic metal ions like lead (Pb) and chromium (Cr) in water.

2. Materials and methods

2.1. Materials

A.R quality zirconium oxychloride and copper sulphate pentahydrate are used as metal sources. Benzene-1,4-dicarboxylic acid (BDC) is used as organic linker. Ethanol is used as solvent. All chemicals were used as received without further treatment.

* Corresponding author.
E-mail address: ranipavithranapril2@gmail.com (R. Pavithran).

https://doi.org/10.1016/j.matpr.2020.05.231
2214-7853/
Selection and peer-review under responsibility of the scientific committee of the International Conference on Energy and Environment.

2.2. Methods

2.2.1. Synthesis of MOF

1 mmol each of metal salt [zirconium oxychloride, copper sulphate pentahydrate] and 1 mmol of BDC were mixed with 10 mL of ethanol. The mixture was transferred into an autoclave and heated at 150 °C for 72 h. It is cooled, filtered and washed with ethanol. The Zr/Cu-BDC MOF was dried in a desiccator over silica crystals.

2.2.2. Characterization methods

Powder X-Ray diffraction data for the prepared MOF was collected on a BRUKER D8 advance X-ray Diffractometer by Cu–Kα radiation with a wavelength of 1.5418 Å at 30 KV and 10 mA. Fourier transform infra-red (FTIR) spectrum was used to detect the functional groups present in the MOF before and after sensing using Perkin Elmer FT-IR spectrophotometer with KBr pellets. Scanning electron microscopy (SEM) images were recorded by Carl Zeiss EVO 18 FE-SEM with EDS. HR-TEM with SAED patterns was taken by using HRTEM: Jeol/JEM 2100. Diffuse reflectance spectra (DRS) were recorded by a UV–Visible Perkin Elmer Lambda 35 spectrophotometer. Luminescence spectra were recorded on a JASCO Spectroflurometer FP-8300. TGA-DTA was taken using Perkin Elmer STA6000.

Table 1
FT-IR spectral data.

Assignment	BDC (cm^{-1})	MOF (cm^{-1})
O-Hstr	3691	3444
=C–H str	3103	2556
C=O stretching	1677	1633, 1682
C–C str aromatics	1573	1510
C–O str	1281	1239
Deformation vibration of benzene	1136, 1018	1018
O–H bend, C–H out of plane aromatics	997, 985	995, 881
CH_2 bend	640	610

2.2.3. Sensing experiments

Potassium dichromate and lead acetate were used as the sources of toxic metal ions. 15 mL of different concentrations; 0.02, 0.04, 0.06, 0.08, 0.1 M of sample solutions were prepared. Small amount of MOF was added to these solutions and mixed well. After mixing the suspension was centrifuged. The residue was collected and used for further analysis. The ability of the MOF for sensing of heavy metal ions from aqueous solution was monitored using UV–vis and PL spectroscopy.

3. Results and discussion

3.1. FT-IR spectral studies

The IR spectra of the ligand 1,4-BDC and of the Zr/Cu-BDC MOF are shown in Fig. 1. In the IR spectrum of MOF broad band observed at 3444 cm^{-1} corresponds to O–H str of BDC. Aromatic-C–H str has been shifted from 3103 cm^{-1} in BDC to lower wave number region at 2556 cm^{-1} in the MOF. C=O stretching band is observed at 1677 in the ligand. Whereas in the MOF, the C=O stretching band is observed as a doublet at 1682 cm^{-1} and at 1633 cm^{-1} indicating the presence of carboxylate group and also the interaction of Zr and Cu with the carboxylate group. The presence of doublet is due to the interaction of two metal ions with oxygen of BDC and also due to hydrogen bonding of C=O bond with the ethanol molecules used during the synthesis [11,12]. Band due to C-O str has been shifted from 1281 cm^{-1} in the ligand to 1239 cm^{-1}. These shifts in IR spectrum suggest the interaction of Zr and Cu to the carboxylate group of the linker in Zr/Cu-BDC MOF (Table 1). The broad band observed at ca. 3450–3000 cm^{-1} in the spectrum of MOF is representative of OH stretching vibrations of ethanol [13].

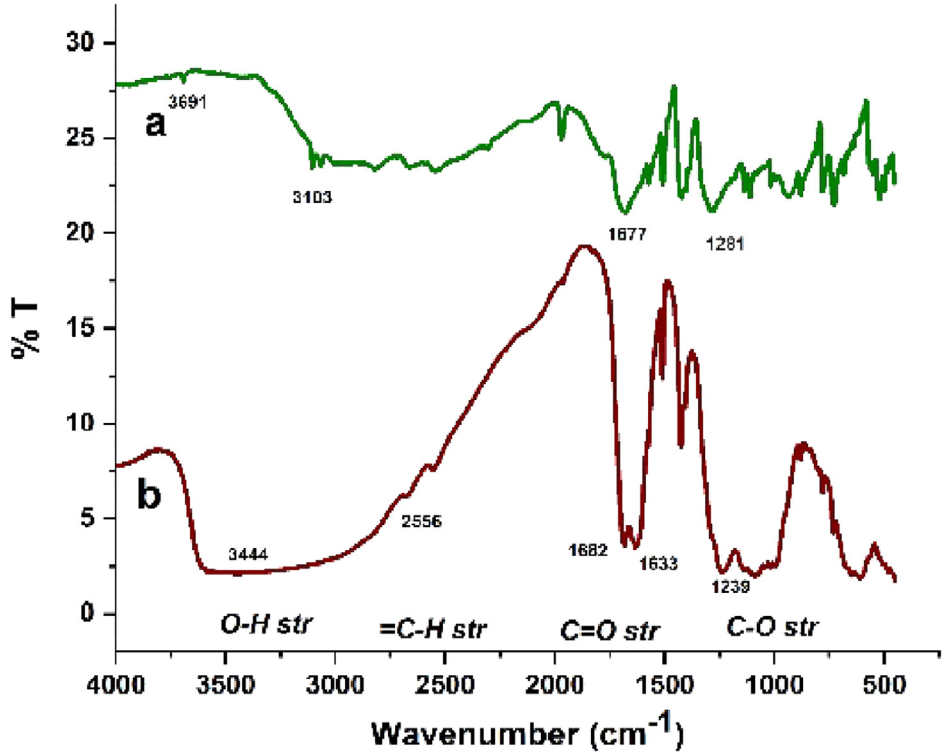

Fig. 1. FT-IR spectra of a) organic linker BDC and b) Zr/Cu-BDC MOF.

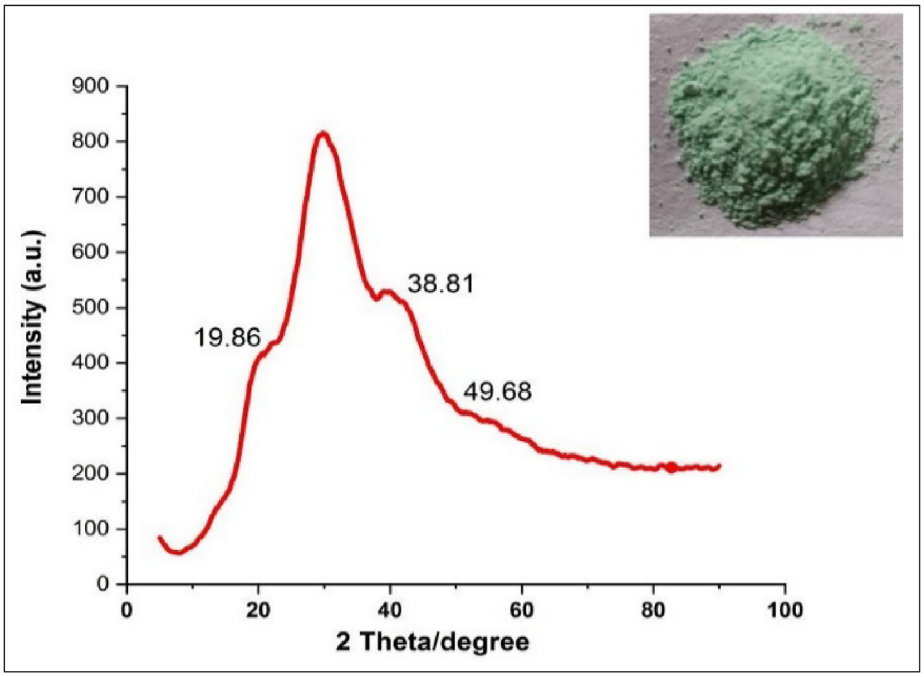

Fig. 2. Powder XRD pattern of Zr/Cu-BDC MOF. Image of MOF powder (inset).

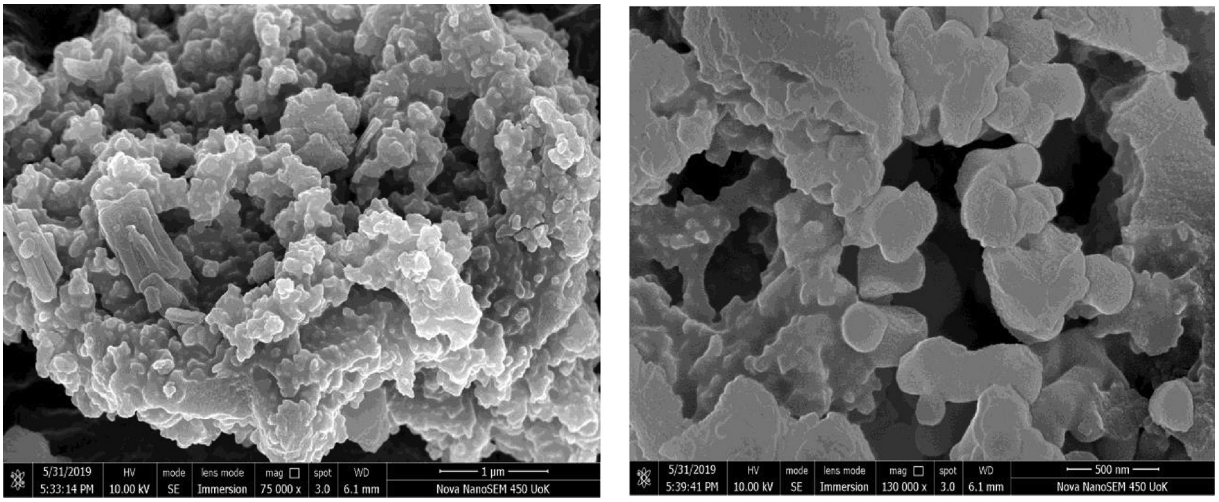

Fig. 3. FE-SEM images of Zr/Cu-BDC MOF.

3.2. Powder X-ray diffraction (PXRD)

Broad peaks at 2θ = 19.86°, 38.81° and 49.68° in the PXRD patterns of MOF indicate a typical amorphous structure without a long range order (Fig. 2).

3.3. FE-SEM analysis

FE-SEM images of Zr/Cu-BDC MOF are shown in Fig. 3. SEM images show coral reef morphology with scale bar 1 μm and 500 nm. The SEM images represent a permanent micro porous framework for Zr/Cu-BDCMOF.

3.4. Energy dispersive spectroscopy (EDS)

Fig. 4 represents the electron dispersive spectrum of the Zr/Cu-BDC MOF. The EDS spectrum shows the presence of Zr and Cu metals, elements like carbon and oxygen present in the linker BDC indicating the successful synthesis of MOF. Table in the EDS spectrum represents the percentage of various elements present in the MOF.

3.5. Thermogravimetric analysis (TGA)

The thermal stability of the MOF was studied by TGA. A small weight loss of MOF at 76.42 °C can be attributed to removal of

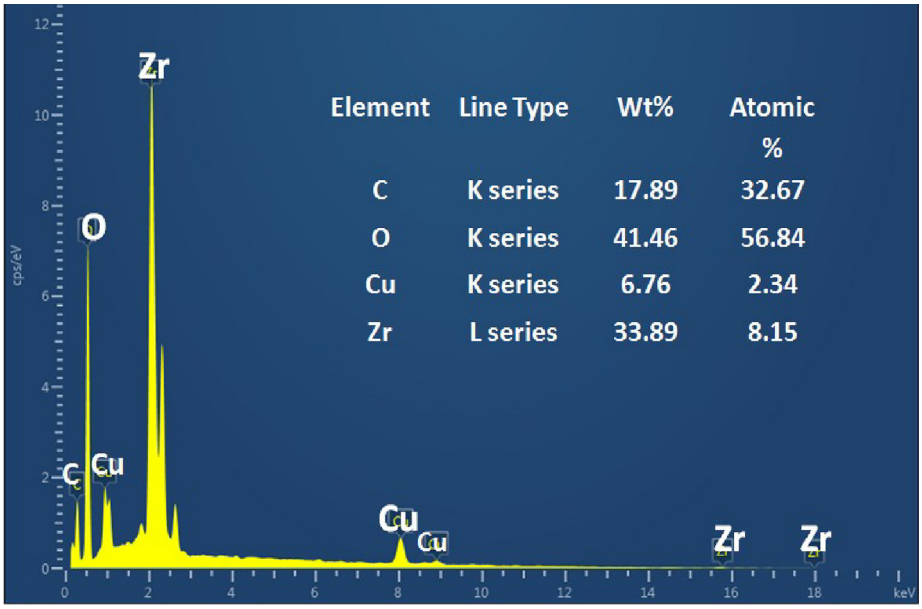

Fig. 4. EDS spectrum of Zr/Cu-BDC MOF.

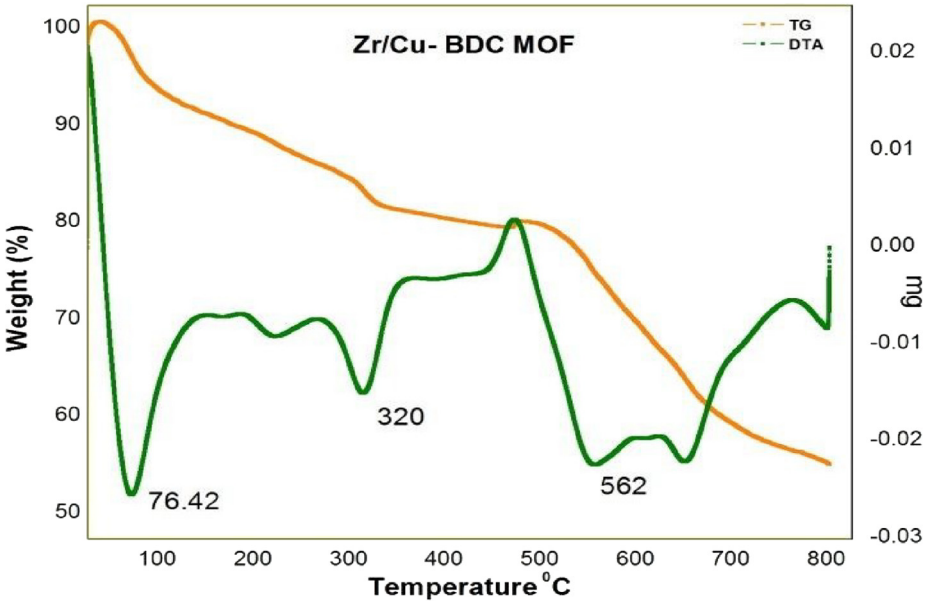

Fig. 5. Thermogram of Zr/Cu-BDC MOF.

moisture and ethanol molecules [14]. The gradual desorption of coordinated ethanol molecules within the pores takes place below 300 °C and the MOF becomes de solvated completely at 320 °C. There after Zr/Cu-BDC MOF is almost stable up to 500 °C. In the temp range of 562 °C complete decomposition of MOF occurs by the breaking of BDC in the framework and the bond breaking of Zr and Cu metals to form residual mass (Fig. 5).

3.6. Diffused reflectance UV–Vis spectra (UV-DRS)

In the UV spectrum of BDC, the absorption band at 301 nm corresponds to n–π* transitions. In the absorption spectrum of Zr/Cu-BDC MOF the absorption band is shifted to lower wavelength region of 290 nm. This may be due to the interaction of the organic chromophore, BDC with copper and zirconium metals via LMCT transition. The band gap of the MOF is calculated from the Tauc plot shown in the inset of Fig. 6 and is found to be 3.57 eV.

3.7. Solid state fluorescence spectra

The solid state emission spectrum of BDC shows emission maximum at 331 nm when excited at 300 nm in Fig. 7 (a). The emission spectra of MOF monitored at various excitation wavelengths are shown in Fig. 7.(b). The emission maxima are observed in the vis-

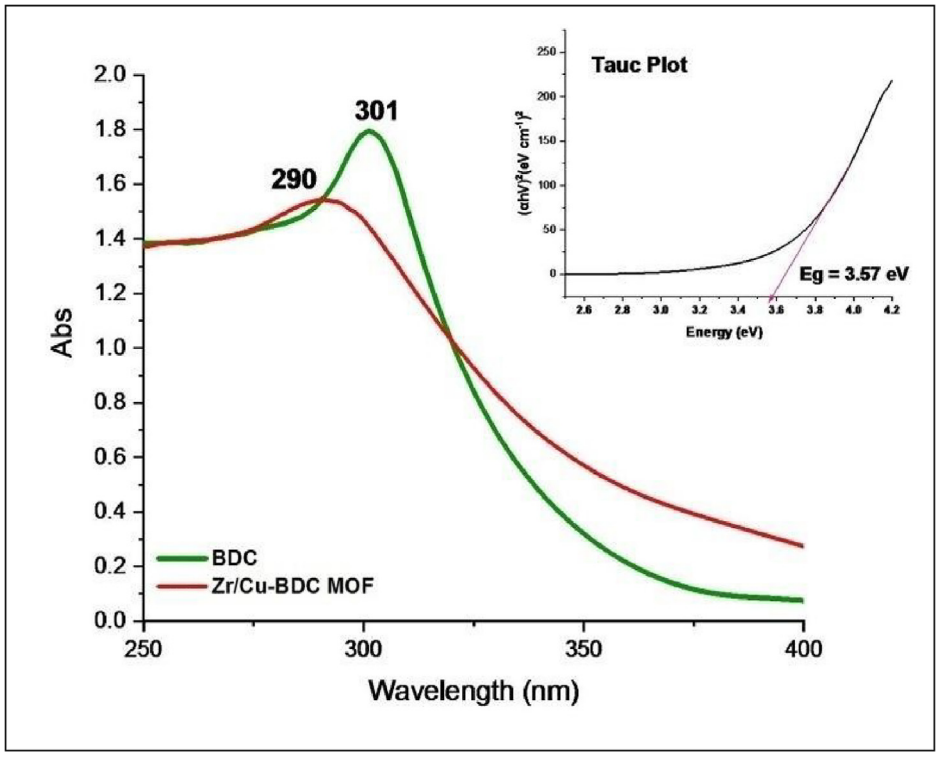

Fig. 6. Diffuse reflectance UV–Vis spectra of BDC and Zr/Cu-BDC MOF. Inset shows the band gap of Zr/Cu-BDC MOF using Tauc plot.

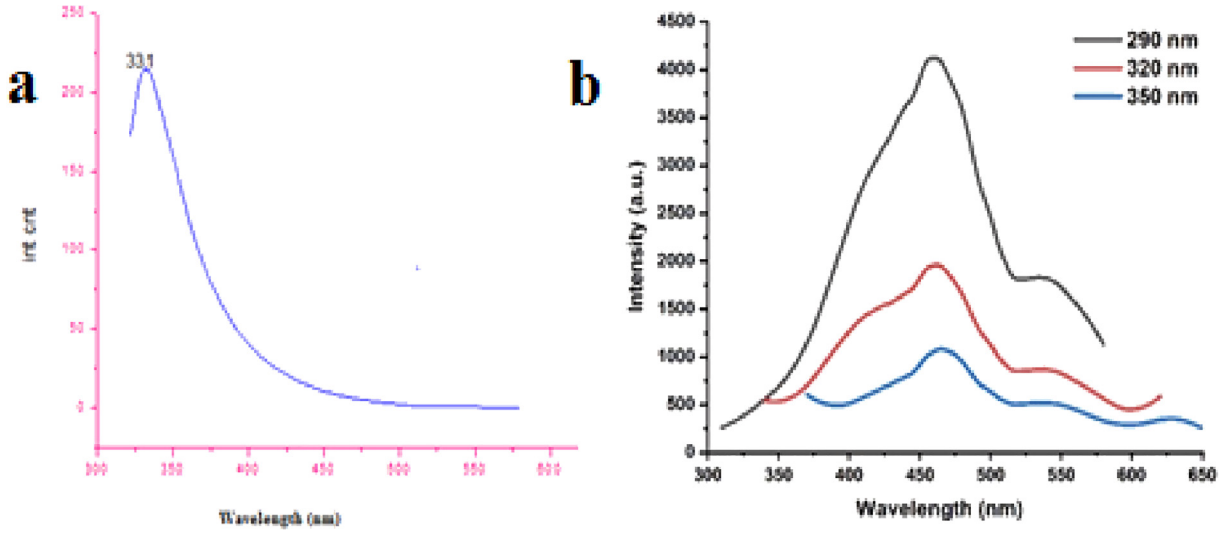

Fig. 7. Solid state emission spectra of a) BDC (b) Zr/Cu-BDC MOF monitored at different excitation wavelengths.

ible region due to the ligand-based emission ($\pi^* \rightarrow \pi$ and $\pi^* \rightarrow$ n transitions) of BDC bonded with the metal ions. The intensity of emission varies with excitation wavelengths and the maximum fluorescence intensity is observed when it is excited at 290 nm.

3.8. Application of MOF in the sensing of toxic metal ions in water

The solutions obtained after conducting sensing experiments were subjected to UV–Visible and Fluorescence Spectral studies. UV–Visible spectrum of MOF alone (Fig. 8) shows absorption maximum at 217 nm due to the $\pi \rightarrow \pi^*$ transition of BDC linker.

Figs. 9 and 10 represent the absorbance spectra monitored after the dispersion of MOF in different concentrations of Pb^{2+} and Cr^{6+} solutions (0.02 M–0.1 M) respectively. The lead solutions exhibit absorption maxima at 327 nm and 341 nm; the chromium solutions exhibit absorption maxima at 234, 314 and 410 nm. Both the metal ions exhibit a red shift in the absorption maxima compared to MOF, which probably accounts for the coordination inter-

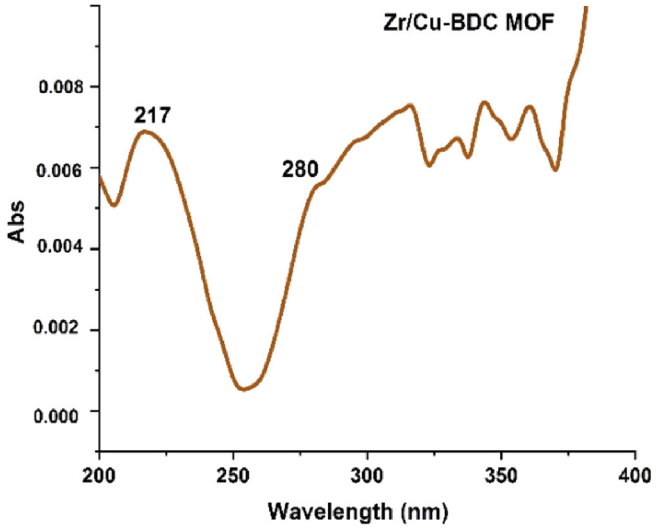

Fig. 8. UV–Visible absorption spectrum of Zr/Cu-BDC MOF.

actions between guest metal ions and the ligand [15]. There is a gradual increase in absorbance with increase in concentrations of lead solution as well as chromium solution.

Fig. 11 shows the fluorescence spectrum of MOF alone excited at 280 nm and that of a mixture of MOF with lead solutions of different concentrations, when excited at 260 nm. The fluorescence intensity is gradually enhanced with increase in concentration of Pb^{2+} ions in water. Thus in the sensing Pb^{2+} ions in water MOF acts as a turn-on sensor [16,17].

Fig. 12 shows the concentration-dependent luminescence spectra of MOF with chromium solutions when excited at 415 nm. The fluorescence spectrum of MOF alone obtained when excited at 240 nm is also shown. The fluorescence intensity of the MOF is gradually quenched with increase in the concentration of chromium (VI) ions from 0.02 to 0.08 M. The shift in the emission maxima to the visible region and the decrease in luminescence intensity with increase in concentration of Cr^{6+} ions in water may be due to luminescent response with ligand–analyte interactions and ligand–to metal charge transfer (LMCT) transitions in MOF [18]. Thus in the sensing of Cr^{6+} ions in water, MOF acts as a turn-off sensor.

3.9. TEM analysis

HR TEM and SAED pattern of MOF before and after sensing Cr (VI) ion is shown (Figs. 13 & 14) respectively. In Fig. 13 (a) the granular shaped MOF is shown, within the surface of framework no metal ions are seen. The TEM images taken after sensing experiments show that chromium ions are adsorbed into the MOF. Dark bright spots confirm the incorporation of toxic Cr^{6+} ion onto the MOF (Fig. 13 (b,c,d))[19].

Diffused rings are observed in the selected area diffraction (SAED) pattern of the MOF (Fig. 14(a)) indicating the amorphous nature MOF. The nature of hetero bimetallic MOF obtained from the powder XRD diffraction patterns are in close agreement with the TEM studies. Fig. 14 (b) represents the SAED pattern of MOF after the sensing experiments. The intensity of diffused rings is higher in Fig. 14 (b) than that in Fig. 14 (a) which may be due to the incorporation of Cr^{6+} ions on the surface of MOF after sensing. The high degree of adsorption of the metal ion on the surface resulted in a high degree of sensing of Cr^{6+} ions in water.

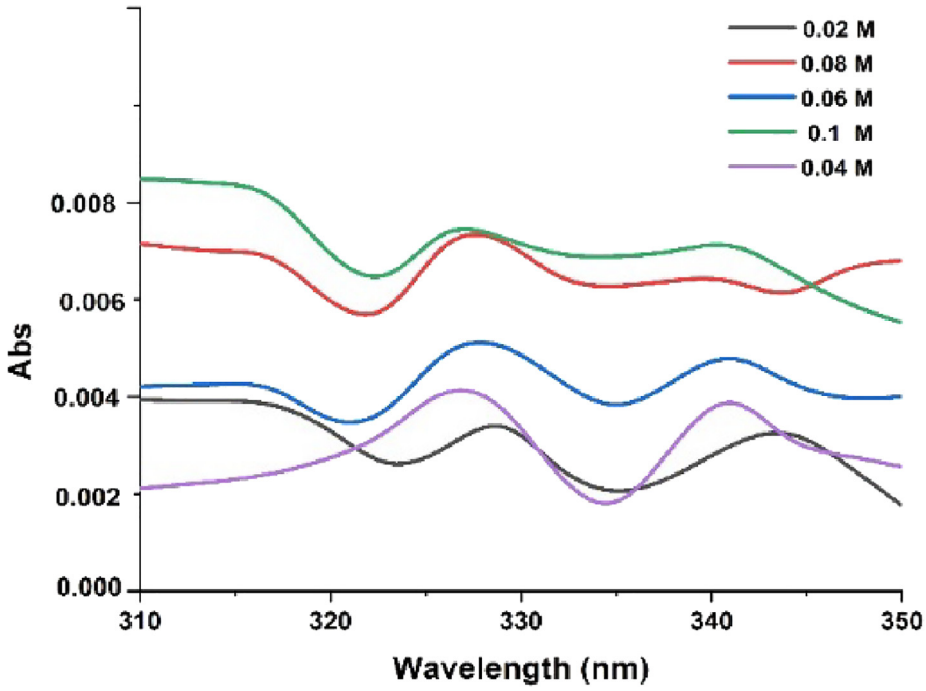

Fig. 9. UV–Visible absorption spectra of Zr/Cu-BDC MOF dispersed in different concentrations of Pb^{2+} in water.

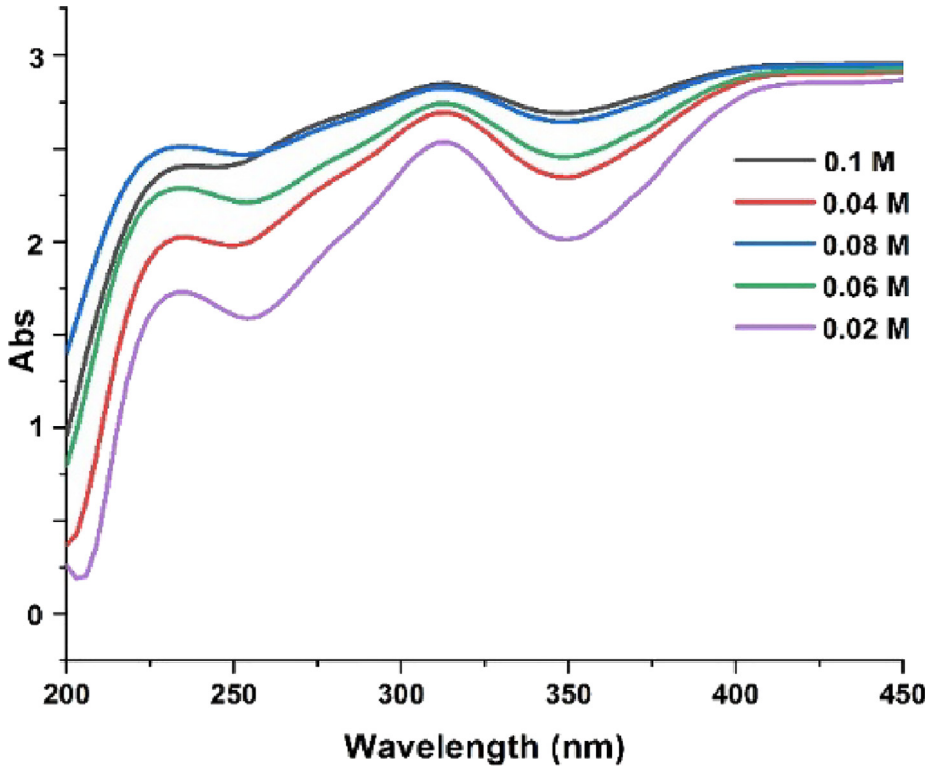

Fig. 10. UV–Visible absorption spectra of Zr/Cu-BDC MOF dispersed in different concentrations of Cr^{6+} in water.

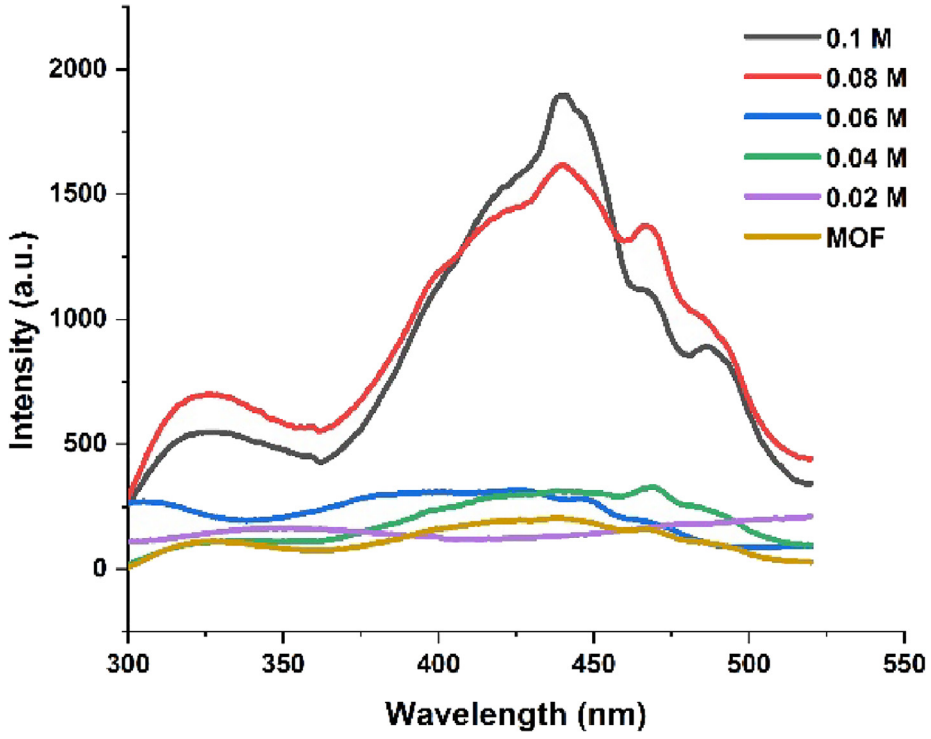

Fig. 11. Fluorescence spectra of Zr/Cu-BDC MOF alone and MOF immersed in different concentrations of Pb^{2+} ions in water.

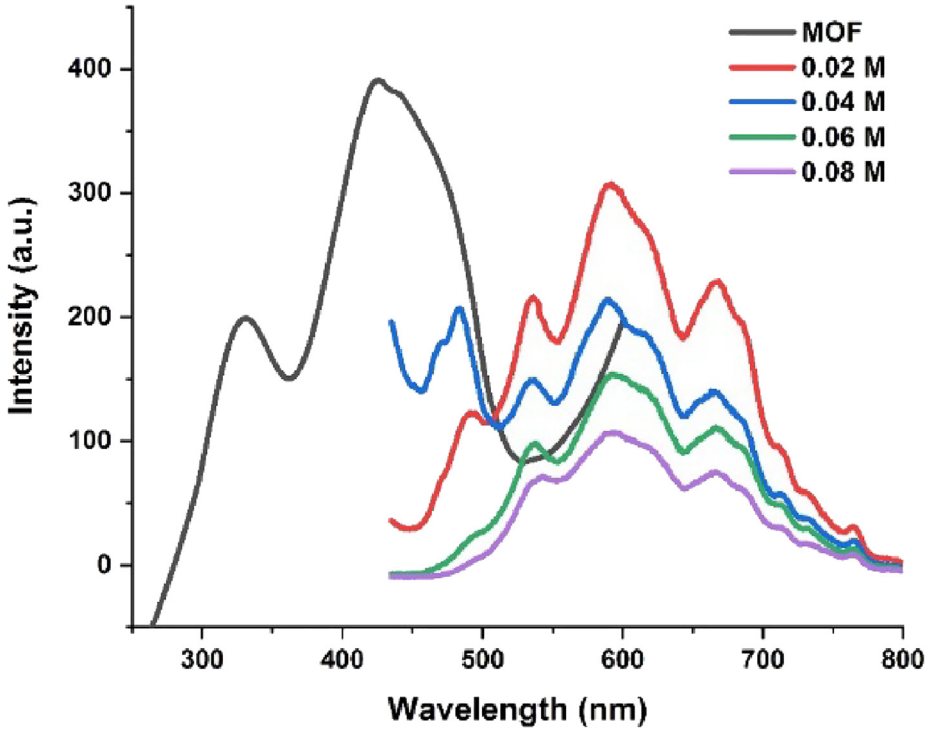

Fig. 12. Fluorescence spectra of Zr/Cu-BDC MOF alone and MOF immersed in different concentrations of Cr^{6+} ions in water.

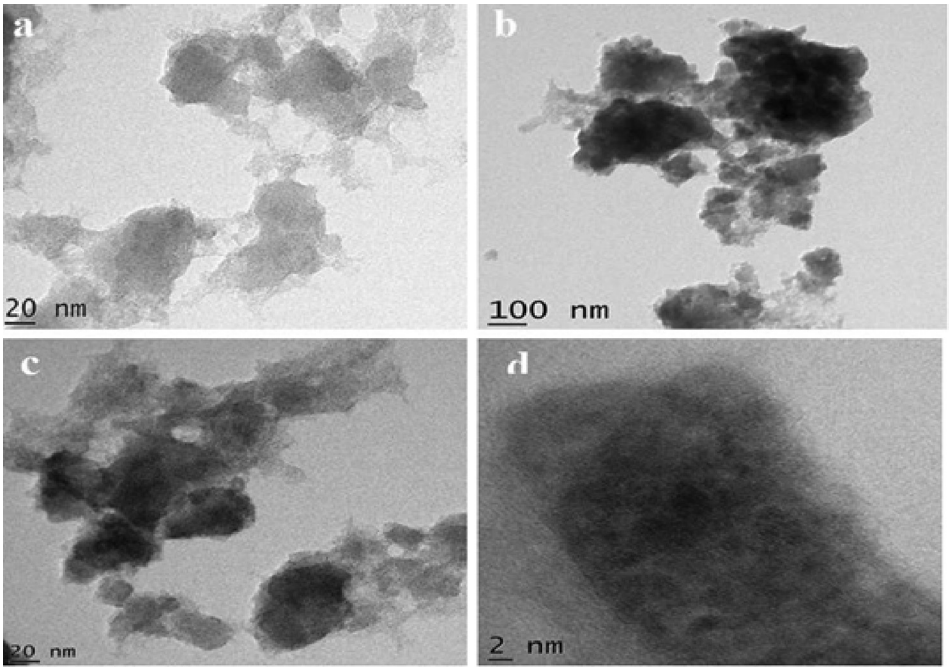

Fig. 13. FE-TEM images of Zr/Cu-BDC MOF (a) before sensing and (b, c, d) after sensing Cr (VI) ion under different magnifications.

The incorporation of Pb^{2+} and Cr^{6+} within the framework of MOF was confirmed from energy dispersive spectra. EDS analysis was done using the residue obtained after conducting sensing experiments and elemental maps are presented in Fig. 15.

3.10. FT-IR spectral data after sensing experiments

FT-IR spectra (Fig. 16) show the bonding characteristics of MOF after the sensing of toxic metal ions in water. The sharp bands at

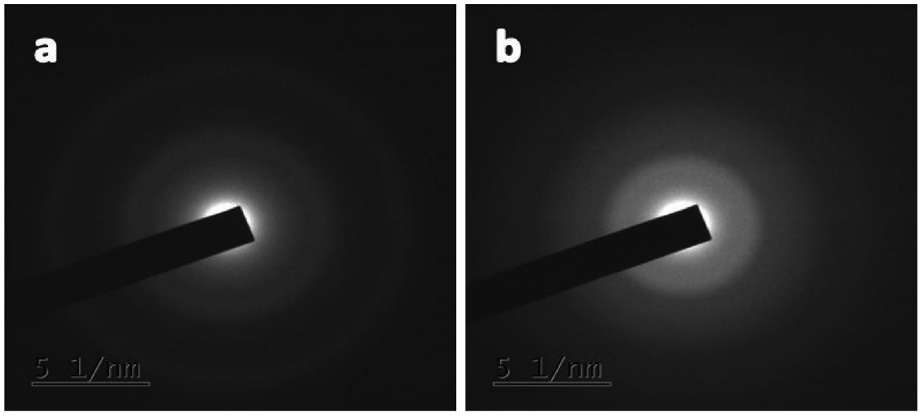

Fig. 14. SAED patterns of (a) Zr/Cu-BDC MOF (b) MOF after sensing Cr(VI) ions.

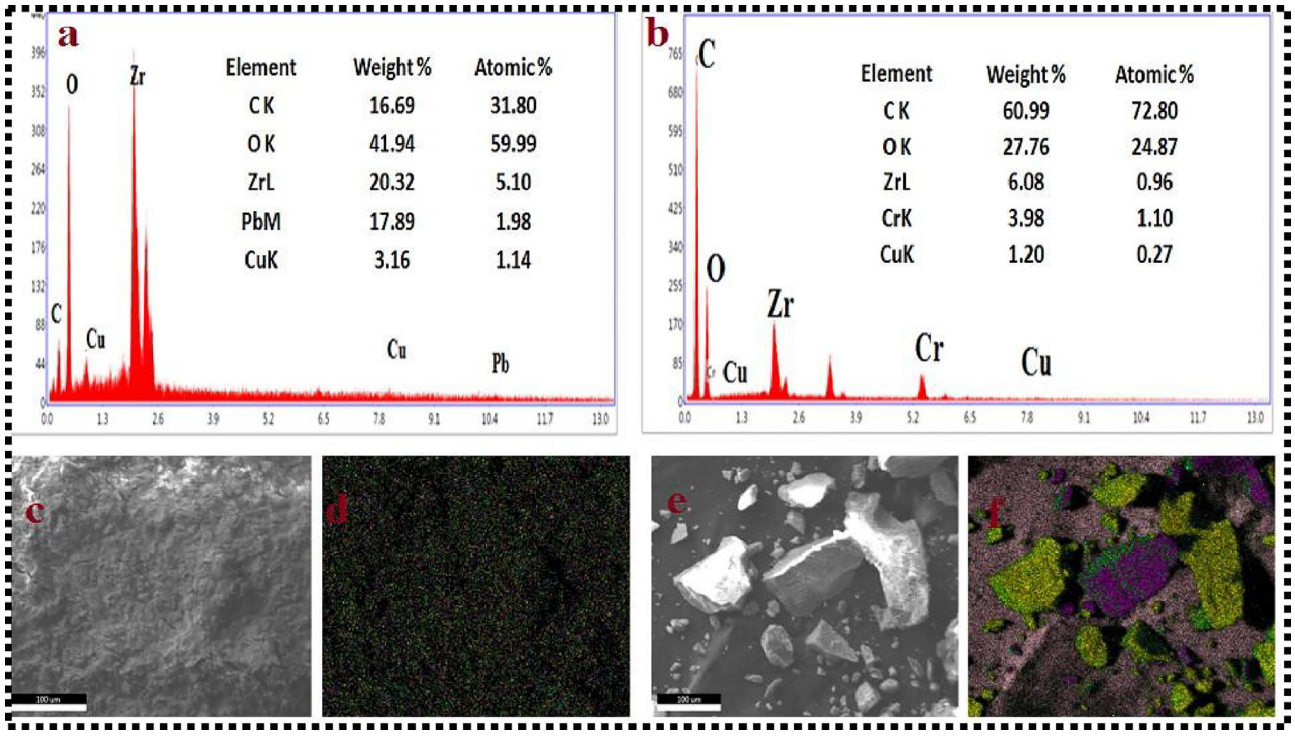

Fig. 15. EDS spectra of MOF after sensing Pb^{2+} (a) and Cr^{6+} (b) ions in water, images c, d, e and f represent the elemental mapping of metal ions.

500–600 cm^{-1} show that Pb^{2+} (590 cm^{-1}) and chromium ions (648 cm^{-1}) are coordinated to the free carboxylate group of the linker [20]. These results suggest the strong interaction between the heavy metal ions (Pb^{2+} and Cr^{6+}) with BDC in MOF after adsorption [21]. IR data confirm that the MOF retains its structural integrity after the interaction of metal ions in aqueous medium, where it is intended to be used as a sensor [22].

3.11. Powder XRD after sensing experiments

Broad peaks in the region $2\theta = 20–50^{\circ}$ suggest the amorphous nature of MOF. The nature of MOF was not changed even after conducting sensing experiments with Pb(II) and Cr(VI) ions in water indicating the chemical stability of the MOF even after the experiments [23] (Fig. 17).

4. Conclusions

We have successfully synthesized a novel amorphous heterobimetallic luminescent MOF of zirconium and copper with benzene-1,4-dicarboxylic acid. It exhibits two types of fluorescence responses with toxic metal ions Pb^{2+} and Cr^{6+}; turn-on sensor with Pb^{2+} ions and turn-off sensor with Cr^{6+} ions in aqueous medium. Heterobimetallic MOFs can be fine-tuned to produce chemo sensitive material responses to specific metal ions. The MOF retains its structural characteristics even after the sensing experiments.

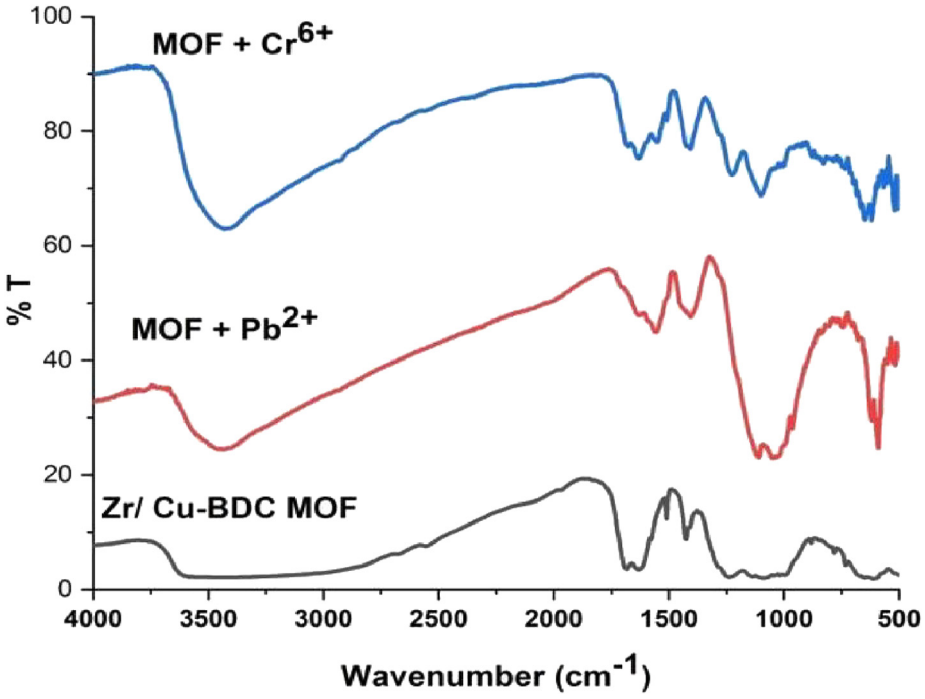

Fig. 16. FT-IR spectra of as synthesized MOF, MOF after sensing of Pb^{2+} ion and MOF after sensing of Cr^{6+} ion.

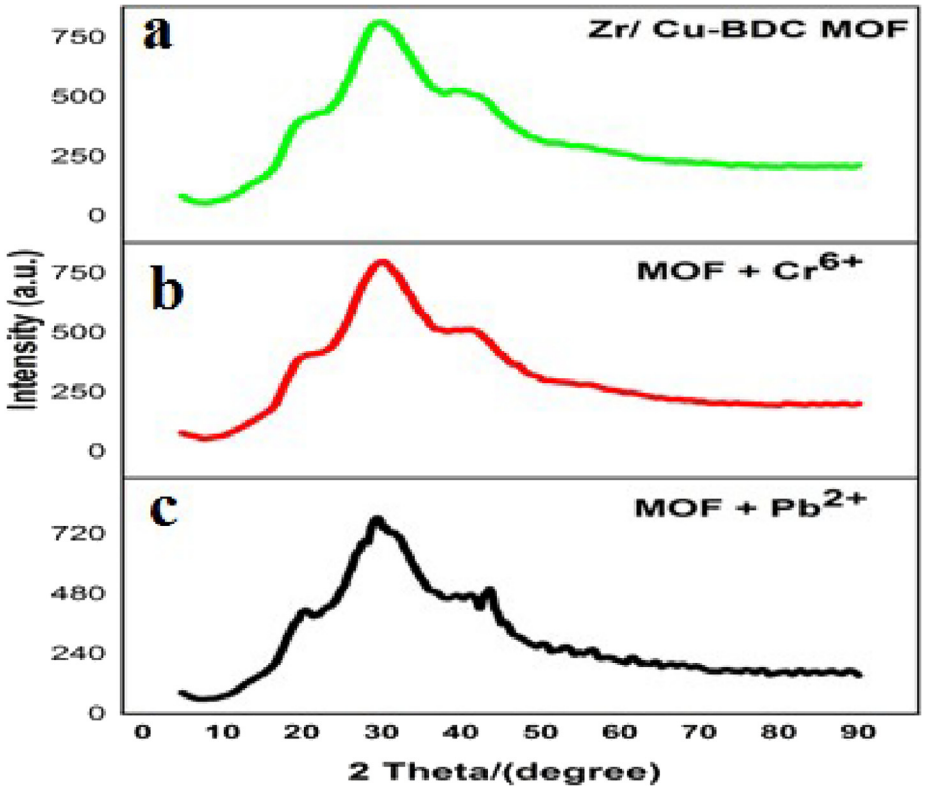

Fig. 17. PXRD patterns of (a) as synthesized MOF (b) MOF after sensing of Cr^{6+} ion(c) after sensing of Pb^{2+} ion.

CRediT authorship contribution statement

M.S. Sreevidya: Investigation, Writing - original draft. **Rani Pavithran:** Conceptualization, Methodology, Validation, Writing - review & editing, Supervision.

Declaration of Competing Interest

The authors declare that they have no known competing financial interests or personal relationships that could have appeared to influence the work reported in this paper.

Acknowledgements

The authors acknowledge the facilities provided by the Department of Chemistry, University College, Thiruvananthapuram, Kerala. The author Ms. Sreevidya M.S. thanks University of Kerala for the financial support in the form of University Research Fellowship.

References

[1] A.D. Pournara, A. Margariti, G.D. Tarlas, A. Kourtelaris, V. Petkov, C. Kokkinos, A. Economou, G.S. Papaefstathiou, M.J. Manos, J. Mater. Chem. A 7 (2019) 15432–15443.
[2] J. Liu, Y. Ye, X. Sun, B. Liu, G. Li, Z. Liang, Y. Liu, J. Mater. Chem. A 7 (2019) 16833–16841.
[3] N.D. Rudd, H. Wang, M.A. Erika, F. Fernandez, S.J. Teat, F. Chen, G. Hall, Y.J. Chabal, J. Li, ACS Appl. Mater. Interfaces 44 (2016) 30294–30303.
[4] W. Liu, Y. Wang, Z. Bai, Y. Li, Y. Wang, L. Chen, L. Xu, J. Diwu, Z. Chai, S. Wang, ACS Appl. Mater. Interfaces 9 (2017) 16448–16457.
[5] Z.Q. Yao, G.Y. Li, J. Xu, T.L. Hu, X.H. Bu, Chem. Eur. J. 24 (2018) 1–8.
[6] R.B. Lin, S.Y. Liu, J.W. Ye, X.Y. Li, J.P. Zhang, Adv. Sci. 3 (2016) 1500434.
[7] D.F. Sava Gallis, Lauren E.S. Rohwer, M.A. Rodriguez, T.M. Nenoff, Chem. Mater. 26 (2014) 2943–2951.
[8] J. Zhang, L. Gong, J. Feng, J. Wu, C. Zhang, New J. Chem. 41 (2017) 8107–8117.
[9] P. Ramaswamy, N.E. Wong, K.H. George Shimizu, Chem. Soc. Rev. 43 (2014) 5913–5932.
[10] B. Wang, Q. Yang, C. Guo, Y. Sun, L.H. Xie, J.R. Li, ACS Appl. Mater. Interfaces 9 (2017) 10286–10295.
[11] N.R. Dhumal, M.P. Singh, J.A. Anderson, J. Kiefer, H.J. Kim, J. Phys. Chem. C 120 (2016) 3295–3304.
[12] K. Tan, N. Nijem, P. Canepa, Q. Gong, J. Li, T. Thonhauser, Y.J. Chabal, Chem. Mater. 16 (2012) 3153–3167.
[13] F. Farzaneh, S. Haghshenas, Mater. Sci. Appl. 3 (2012) 697–703.
[14] B. Zhang, J. Zhang, C. Liu, X. Sang, L. Peng, X. Ma, T. Wu, B. Han, G. Yang, RSC Adv. 5 (2015) 37691–37696.
[15] C.X. Yang, H.B. Ran, X.P. Yan, Anal. Chem. 85 (2013) 7441–7446.
[16] M.H. Yu, T.L. Hu, X.H. Bu, Inorg. Chem. Front. 4 (2017) 256–260.
[17] A. Karmakar, P. Samanta, S. Dutta, S.K. Ghosh, Chem. Chem Asian J. 24 (2019) 4506–4519.
[18] Y. Hao, S. Chen, Y. Zhou, Y. Zhang, M. Xu, Nanomaterials 9 (2019) 974.
[19] C. Wiktor, M. Meledina, S. Turner, O.I. Lebedevd, R.A. Fischer, J. Mater. Chem. A 5 (2017) 14969–14989.
[20] S. Zhao, J. Yang, Y.Y. Liu, J.F. Ma, Inorg. Chem. 55 (2016) 2261–2273.
[21] F. Yi, D. Chen, M. Wu, L. Han, H.L. Jiang, ChemPlusChem 81 (2016) 675–690.
[22] L. Han, L. Qin, L. Xu, Y. Zhou, J. Sun, X. Zou, Chem. Commun. 49 (2013) 406.
[23] M.A. Ali, J. Ren, T. Zhao, X. Liu, Y. Hua, Y. Yue, J. Qiu, ACS Omega 4 (2019) 12081–12087.